

Synthesis, crystal structure and spectroscopic properties of a novel yttrium(iii) fluoride dimolybdate(vi): YFMo₂O₇

Ingo Hartenbach, Henning A. Höpfe, Karolina Kazmierczak, Thomas Schleid

Angaben zur Veröffentlichung / Publication details:

Hartenbach, Ingo, Henning A. Höpfe, Karolina Kazmierczak, and Thomas Schleid. 2014. "Synthesis, crystal structure and spectroscopic properties of a novel yttrium(iii) fluoride dimolybdate(vi): YFMo₂O₇." Dalton Transactions 43 (37): 14016–21. <https://doi.org/10.1039/c4dt01066c>.

Nutzungsbedingungen / Terms of use:

licgercopyright

Dieses Dokument wird unter folgenden Bedingungen zur Verfügung gestellt: / This document is made available under these conditions:

Deutsches Urheberrecht

Weitere Informationen finden Sie unter: / For more information see:

<https://www.uni-augsburg.de/de/organisation/bibliothek/publizieren-zitieren-archivieren/publiz/>



Synthesis, crystal structure and spectroscopic properties of a novel yttrium(III) fluoride dimolybdate(VI): YFMo_2O_7 †

Ingo Hartenbach,^{*a} Henning A. Höpfe,^b Karolina Kazmierczak^b and Thomas Schleid^a

Thermal treatment of a mixture of Y_2O_3 , YF_3 and MoO_3 in a 1:1:6 molar ratio at 850 °C in evacuated silica ampoules yielded colorless, platelet-shaped single crystals of YFMo_2O_7 . SiO_2 was dissolved from the ampoule wall in small amounts, but could be removed from the crude product by treatment with hydrofluoric acid (20%). The title compound crystallizes monoclinically in the space group $P2_1/c$ with two formula units per unit cell with the dimensions $a = 4.2609(2)$, $b = 6.5644(4)$, $c = 11.3523(7)$ Å, and $\beta = 90.511(2)^\circ$. Its crystal structure contains crystallographically unique Y^{3+} cations in a pentagonal bipyramidal environment consisting of two F^- anions in the apical positions and five O^{2-} anions in the equatorial positions. These polyhedra are connected to ${}_{\infty}^1\{\{\text{YF}_{2/2}\text{O}_{5/1}^{\dagger}\}^{\text{B}^-}\}$ chains along [100] by sharing common F^- vertices. The likewise crystallographically unique Mo^{6+} cations exhibit a coordination number of five and reside in the centers of distorted square pyramids built up of oxide anions. These entities are fused to chains along [001] by sharing common edges and vertices according to ${}_{\infty}^1\{\{\text{MoO}_{2/2}\text{O}_{1/2}\text{O}_{2/1}^{\dagger}\}^{\text{B}^-}\}$. Taking a sixth oxygen ligand further away from the Mo^{6+} cations into account, the aforementioned chains assemble to corrugated ${}_{\infty}^2\{\{\text{MoO}_{2/2}\text{O}_{3/2}\text{O}_{1/1}^{\dagger}\}^{\text{B}^-}\}$ layers perpendicular to [010] with the ${}_{\infty}^1\{\{\text{YF}_{2/2}\text{O}_{5/1}^{\dagger}\}^{\text{B}^-}\}$ chains situated between these sheets. Since Y^{3+} represents a non-luminescent rare-earth metal(III) cation, YFMo_2O_7 is a suitable host material for doping with luminescence-active lanthanoid(III) cations, such as Eu^{3+} .

Introduction

The quest for energy efficient materials has been a major topic of scientific research for over a decade. This includes the search for compounds, which display the ability to convert invisible electromagnetic radiation into visible light. In the past, oxido-molybdates(VI) of yttrium (e.g. $\text{Y}_2[\text{MoO}_4]_3$ and $\text{Y}_2[\text{MoO}_4]_2[\text{Mo}_2\text{O}_7]^{1-}$ and their fluoride derivatives (e.g. $\text{YF}[\text{MoO}_4]^{2-}$) have proven to be suitable host materials for luminescence applications. The most interesting fact about these classes of compounds is the ability of the oxido-molybdate(VI) groups to harvest light from the UV region of the spectral band utilizing their ligand-to-metal charge transfer (LMCT) process and subsequently transfer this energy to a luminescence-active cation, such as Eu^{3+} or Tb^{3+} , causing them to emit visible light. If the structure contains only discrete tetrahedral *ortho*-oxido-molybdate(VI) entities $[\text{MoO}_4]^{2-}$, the LMCT energy is located at

about 290 nm.³ By altering the size of these units to dimolybdate(VI) pyroanions¹ $[\text{Mo}_2\text{O}_7]^{2-}$ or higher aggregated entities, it is possible to shift this wavelength towards an area of lower energy. Besides the aforementioned $\text{O}^{2-} \rightarrow \text{Mo}^{6+}$ LMCT, the $\text{O}^{2-} \rightarrow \text{Eu}^{3+}$ charge transfer process has to be taken into account as well, although the latter strongly depends on the coordination environment of the europium(III) cations in the actual crystal structure. The title compound YFMo_2O_7 represents the first fluoride-derivatized yttrium(III) oxido-molybdate(VI) with an extended molybdate substructure, in which the coordination spheres of the central molybdenum(VI) cations are enlarged and no isolated $[\text{Mo}_2\text{O}_7]^{2-}$ pyroanions are present. This increase of the coordination number for Mo^{6+} is observed for quite a few compounds, e.g. C.N. = 5, represented by isolated $[\text{MoO}_5]^{4-}$ anions in $\text{Ce}_2[\text{MoO}_4][\text{MoO}_5]$,⁴ or C.N. = 6, found as edge-sharing $[\text{MoO}_6]^{6-}$ octahedra in Keggin-type anions as in $\text{H}_3[\text{PMo}_{12}\text{O}_{40}] \cdot 6\text{H}_2\text{O}$,⁵ for example.

Experimental

Synthesis

YFMo_2O_7 was obtained from a mixture of yttrium sesquioxide (Y_2O_3 : 99.9%; ChemPur, Karlsruhe, Germany), yttrium

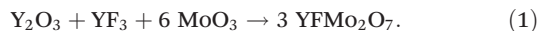
^aInstitute for Inorganic Chemistry, University of Stuttgart, Pfaffenwaldring 55, 70569 Stuttgart, Germany. E-mail: hartenbach@iac.uni-stuttgart.de;

Fax: +49(0)711/685-64254

^bInstitute for Physics, University of Augsburg, Universitätsstr. 1, 86159 Stuttgart, Germany

†Electronic supplementary information (ESI) available: Crystal information file. See DOI: 10.1039/c4dt01066c

trifluoride (YF₃: 99.9%; ChemPur, Karlsruhe, Germany), and molybdenum trioxide (MoO₃: *p.a.*; Merck, Darmstadt, Germany) in a 1 : 1 : 6 molar ratio, which was heated at 850 °C for six days in evacuated silica ampoules according to eqn (1):



From this reaction colorless, transparent, and platelet-shaped crystals of the title compound were obtained, which remained stable in air and water, while a shorter reaction time only yields a microcrystalline crude product. The use of fluoride anions from YF₃ resulted in a minor impurity of SiO₂ in the crude product, which was dissolved from the ampoule wall and recrystallized to α -cristobalite-type silicon dioxide. This undesired by-product could be removed by treatment of the reaction products with an aqueous solution of hydrofluoric acid (20%), which transformed the SiO₂ component into soluble [SiF₆]²⁻ or SiF₄ and silicon oxide fluorides, which are volatile at room temperature. The remaining product was unharmed by this procedure and could be identified as single-phase YFMo₂O₇ according to X-ray powder diffraction (Fig. 1). In order to synthesize Eu³⁺-doped samples, about 2% of the yttrium sesquioxide was replaced by europium sesquioxide (Eu₂O₃: 99.9%; ChemPur, Karlsruhe, Germany) in the reactant mixture, while the reaction conditions as well as the rinsing treatment of the crude product remained the same as for the undoped compound. Synthesis routes which are more energy efficient, such as solvochemical procedures, have proven to be unsuccessful so far.

X-ray crystallography

The X-ray powder patterns were measured on a Stoe STADI P diffractometer with a position-sensitive detector using germanium-monochromatized Cu-K α radiation (wavelength: $\lambda = 1.5406$ Å, step size 0.1°, irradiation time 60 s). The refinement of the powder diffractogram (Fig. 1) was performed with the help of the program FULLPROF (Version 2K²) implemented in the WINPLOTR program suite.⁶ Deviations of intensities

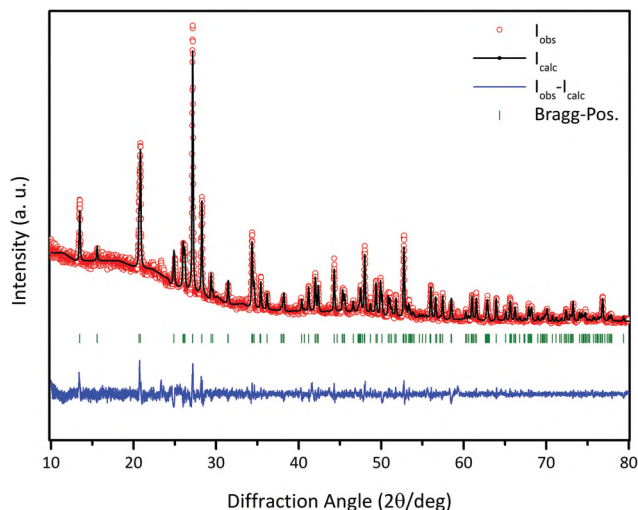


Fig. 1 X-ray powder diffractogram of single phase YFMo₂O₇.

within the powder diffractogram are due to texture effects of the mostly platelet-shaped microcrystals.

Intensity datasets for single crystals of YFMo₂O₇ were collected on a Nonius Kappa-CCD diffractometer using graphite-monochromatized Mo-K α radiation (wavelength: $\lambda = 0.7107$ Å, φ - and ω -scans, irradiation time: 20 s per degree). Numerical absorption correction was carried out with the help of the program HABITUS,⁷ and structure solution and refinement were performed with the program suite SHELX-97.⁸ Details of the data collection and the structure refinement⁹ are summarized in Table 1; atomic positions and coefficients of the isotropic thermal displacement parameters¹⁰ are shown in Table 2; and motifs of mutual adjunction¹¹ as well as interatomic distances are given in Table 3. Further details of the crystal structure investigation are available from the Fachinformationszentrum (FIZ) Karlsruhe, D-76344 Eggenstein-Leopoldshafen, Germany (Fax: +49(0)7247-808-444; e-mail: crysdata@fiz-karlsruhe.de), on quoting the depository number CSD 427022 for YFMo₂O₇.

Table 1 Crystallographic data for YFMo₂O₇

Empirical formula	YFMo ₂ O ₇
Crystal system; space group	monoclinic; <i>P2/c</i> (no. 13)
Formula units	<i>Z</i> = 2
Lattice constants, <i>a</i> /Å	4.2609(2)
<i>b</i> /Å	6.5644(4)
<i>c</i> /Å	11.3523(7)
β /°	90.511(2)
Calculated density, <i>D_x</i> /g cm ⁻³	4.307
Molar volume, <i>V_m</i> /cm ³ mol ⁻¹	95.605
<i>F</i> (000); absorption coefficient, μ /mm ⁻¹	376; 12.963
Index range ($\pm h/\pm k/\pm l$)	5/8/15
Theta range ($\theta_{\min} - \theta_{\max}$)	3.10–28.25
Data corrections	Background, polarization and Lorentz factors; numerical absorption correction with the program HABITUS ⁷
Collected/unique reflections/free parameters	7716/797/54
<i>R_{int}</i> / <i>R_σ</i>	0.087/0.031
<i>R₁</i> for $ F_o \geq 4\sigma(F_o)$ reflections with $ F_o \geq 4\sigma(F_o)$	0.021/795
<i>R₁</i> / <i>wR₂</i> for all reflections	0.021/0.053
Goodness of fit (GooF)	1.088
Extinction coefficient, <i>g</i>	0.071(3)
Residual electron density, $\rho/e^- \times 10^{-6}$ pm ⁻³	max.: 0.79, min.: -0.82

Table 2 Atomic coordinates and equivalent isotropic displacement factors *U_{eq}*^a for YFMo₂O₇

Atom	Wyckoff position	<i>x/a</i>	<i>y/b</i>	<i>z/c</i>	<i>U_{eq}</i> /Å ²
Y	2 <i>e</i>	0	0.79522(8)	1/4	0.0083(2)
F	2 <i>f</i>	1/2	0.8035(6)	1/4	0.0280(9)
Mo	4 <i>g</i>	0.09830(7)	0.33053(5)	0.09409(3)	0.0097(1)
O1	4 <i>g</i>	0.4972(7)	0.3428(4)	0.0972(3)	0.0181(6)
O2	4 <i>g</i>	0.0164(7)	0.0778(4)	0.1271(2)	0.0170(6)
O3	4 <i>g</i>	0.0026(7)	0.6498(4)	0.0663(2)	0.0135(5)
O4	2 <i>e</i>	0	0.4389(6)	1/4	0.0121(7)

^a *U_{eq}* is defined as 1/3 of the trace of the orthogonalized *U_{ij}* tensor.¹⁰

Table 3 Motifs of mutual adjunction¹¹ and selected interatomic distances (in Å) for YFMo₂O₇

	F	O1	O2	O3	O4	C.N.
Y	2/2 2.131(2)	0/0	2/1 2.323(2)	2/1 2.294(3)	1/1 2.339(4)	7
Mo	0/0	1 + 1/1 + 1 1.701(3) 2.563(3)	1/1 1.737(3)	2/2 1.811(3) 2.158(3)	1/2 1.956(2)	5 + 1
C.N.	2	1 + 1	2	3	3	

IR and Raman spectroscopy

The infrared spectrum of YFMo₂O₇ was recorded on a Thermo Scientific Nicolet iS5 spectrometer equipped with an ATR unit using a diamond crystal measuring the reflection of the powdered sample. Raman spectroscopy was performed with the help of a Thermo Scientific DXR SmartRaman 780 spectrometer using a green excitation laser (wavelength: $\lambda = 780$ nm) for irradiation of the compressed powder sample.

UV-Vis and luminescence spectroscopy

Diffuse reflectance spectra were collected on a J & M TIDAS UV-Vis-NIR spectrophotometer equipped with a reflectance measuring geometry. A barium sulfate standard was used as a white reference and the Kubelka–Munk function was applied to obtain band-gap information.¹² The position of the onset point of the band gap was determined by the intersection of the linear fit at the steepest slope with the linear baseline fit of the spectrum. The maximum of the band gap was determined by the position of the inflection point in the steepest slope within the spectrum. Solid-state excitation and emission spectra were recorded at room temperature using a Horiba FluoroMax-4 fluorescence spectrometer equipped with a xenon discharge lamp scanning the range from 200 to 800 nm. Electronic transitions were assigned according to the energy-level diagrams of trivalent europium cations.¹³

Results and discussion

Crystal structure

YFMo₂O₇ crystallizes monoclinically in the space group *P2/c* ($a = 4.2609(2)$, $b = 6.5644(4)$, $c = 11.3523(7)$ Å, $\beta = 90.511(2)^\circ$) with two formula units per unit cell. The crystallographically unique Y³⁺ cations reside on the Wyckoff position *2e* (symmetry: 2) with pentagonal bipyramids built up by two F⁻ anions representing the apical vertices and five O²⁻ ligands in the equatorial plane as the coordination environment (Fig. 2, left). These [YF₂O₅]⁹⁻ polyhedra share common fluoride vertices to form ${}^1_{\infty}\{[YF_{2/2}O_{5/1}]^{8-}\}$ chains along [100] (Fig. 2, right).

Although the distances between Y³⁺ and F⁻ are unusually short with a value of 2.131(3) Å (2 \times), there are quite a few compounds, *e.g.* Cs₂KYF₆ exhibiting the same short Y³⁺–F⁻ distances of 2.13 Å.¹⁴ The distances between yttrium and oxygen range between 2.29 and 2.34 Å, which is also found in most compounds containing yttrium and oxygen, including in

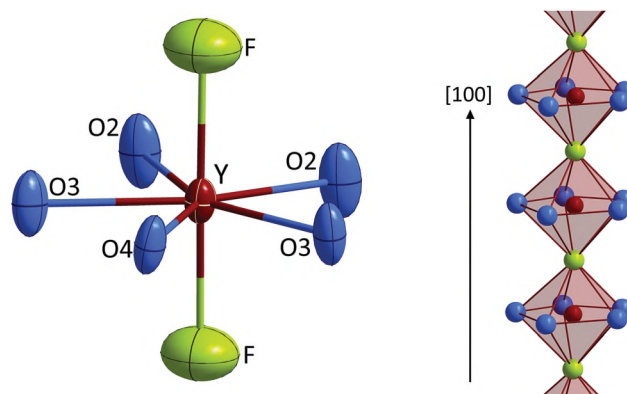


Fig. 2 Coordination environment of the Y³⁺ cations (left) and ${}^1_{\infty}\{[YF_{2/2}O_{5/1}]^{8-}\}$ chains along [100], formed by sharing the fluoride vertices of pentagonal [YF₂O₅]⁹⁻ bipyramids in the crystal structure of YFMo₂O₇ (ellipsoid representation at 95% probability).

bixbyite-type yttrium sesquioxide (Y₂O₃) itself ($d(Y^{3+}-O^{2-}) = 2.25-2.35$ Å).¹⁵ The crystal structure exhibits crystallographically unique Mo⁶⁺ cations, located at the general Wyckoff position *4g*, which are surrounded by five oxygen atoms in the shape of a distorted square pyramid (Fig. 3, left). The molybdenum–oxygen distances cover a broad range between 1.70 and 2.16 Å. While the shorter distances of 1.70 and 1.74 Å are typical for terminal Mo⁶⁺–O²⁻ contacts as found *e.g.* in K₂[MoO₄], which contains isolated *ortho*-oxidomolybdate(vi) tetrahedra ($d(Mo^{6+}-O^{2-}) = 1.74-1.78$ Å),¹⁶ the larger ones of 1.87–2.16 Å appear common for those representing connective vertices or even parts of linking edges, just like in molybdenum trioxide (MoO₃) itself ($d(Mo^{6+}-O^{2-}) = 1.87-2.45$ Å).¹⁷ The [MoO₅]⁴⁻ pyramids join together to form ${}^1_{\infty}\{[MoO_{2/2}^eO_{1/2}^vO_{2/1}^t]^{-}\}$ (*e* = edge, *v* = vertex, *t* = terminal) chains along [001] *via* common oxide vertices and edges (Fig. 3, right).

The terminal (O1)²⁻ anions display a second, long-distance contact of 2.56 Å to the Mo⁶⁺ cations increasing their coordination number to 5 + 1 and expanding the coordination polyhedra to highly distorted octahedra with eccentrically coordinated Mo⁶⁺ cations (Fig. 3, left). The aforementioned

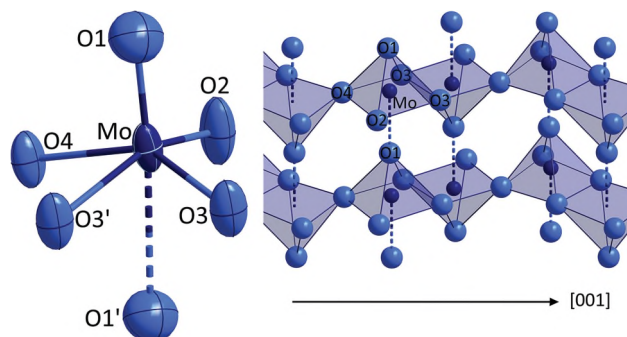


Fig. 3 Coordination environment of the Mo⁶⁺ cations (left, ellipsoid representation at 95% probability), including a sixth fairly long contact (dashed line), and ${}^1_{\infty}\{[MoO_{2/2}^eO_{1/2}^vO_{2/1}^t]^{-}\}$ chains along [001] (right), which are interconnected by the aforementioned extra contact to corrugated ${}^2_{\infty}\{[MoO_{2/2}^eO_{3/2}^vO_{1/1}^t]^{-}\}$ layers parallel to the (010) plane.

$^1_{\infty}\{\text{MoO}_{2/2}\text{O}_{1/2}\text{O}_{2/1}^{\text{I}}\}^-$ strands are subsequently connected to each other, forming corrugated $^2_{\infty}\{\text{MoO}_{2/2}\text{O}_{3/2}\text{O}_{1/1}^{\text{I}}\}^-$ layers perpendicular to the [010] direction (Fig. 3, right). According to ECoN (effective coordination number)¹⁸ calculations the most distant attractive contact (2.56 Å) between Mo^{6+} and $(\text{O}1)^{2-}$ has no contribution to the effective coordination numbers (ECoN) of either atoms; however, the description of the structure can be simplified by taking it into consideration anyhow. Therefore, the crystal structure can be described as if being assembled by layers of the composition $^2_{\infty}\{\text{MoO}_{2/2}\text{O}_{3/2}\text{O}_{1/1}^{\text{I}}\}^-$ spreading out parallel to the (010) plane, between which $^1_{\infty}\{\text{YF}_{2/2}\}^{2+}$ strands are situated running along [100] (Fig. 4).

The monoclinic angle of almost 90° suggests a strong relationship with the orthorhombic crystal system, however a structure solution in an orthorhombic supergroup of $P2/c$ places the Mo^{6+} cations right into the centers of the aforementioned oxygen octahedra. Since the maxima of the electron density in the final structure-refinement cycles remain more than 0.4 Å offset towards one of the $(\text{O}1)^{2-}$ vertices (Fig. 5), mirror planes perpendicular to [100] cannot be postulated seriously, hence only monoclinic symmetry is found.

IR and Raman spectroscopy

The distorted square oxidomolybdate(vi) pyramids $[\text{MoO}_5]^{4-}$ within the $^2_{\infty}\{\text{MoO}_{2/2}\text{O}_{3/2}\text{O}_{1/1}^{\text{I}}\}^-$ layers display merely symmetry 1 (C_1), offering the usual range for stretching vibrations of these pyramidal entities situated in the same area as found for tetrahedral $[\text{MoO}_4]^{2-}$ anions, *i.e.* between 800 and 1000 wavenumbers.¹⁹ In the IR spectrum (Fig. 6, top) two wide peaks, which both appear to be superimposed peaks each, are found between 840 and 980 wavenumbers, typically assignable to Mo–O stretching vibrations with the symmetric one at the highest energy. According to Busca,¹⁹ the Mo–O–Mo stretching vibrations of the vertex-linked regions within the oxidomolybdate(vi) layers can be detected at energies lower than 800 wave-

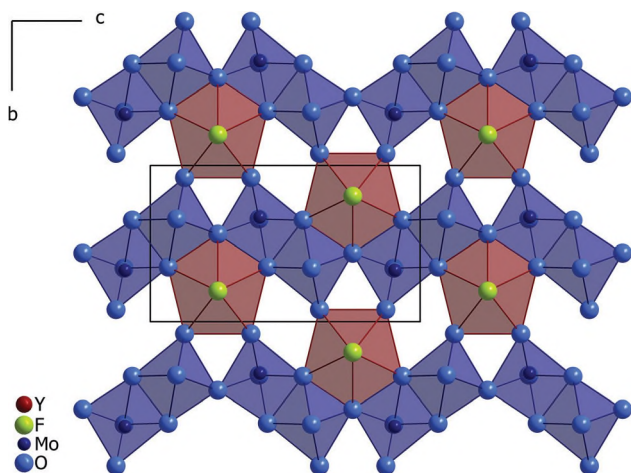


Fig. 4 View at the crystal structure of YFMO_2O_7 along the a -axis. The structure can be described as being built up by $^2_{\infty}\{\text{MoO}_{2/2}\text{O}_{3/2}\text{O}_{1/1}^{\text{I}}\}^-$ layers (represented by blue polyhedra) and $^1_{\infty}\{\text{YF}_{2/2}\}^{2+}$ strands (within the red polyhedra).

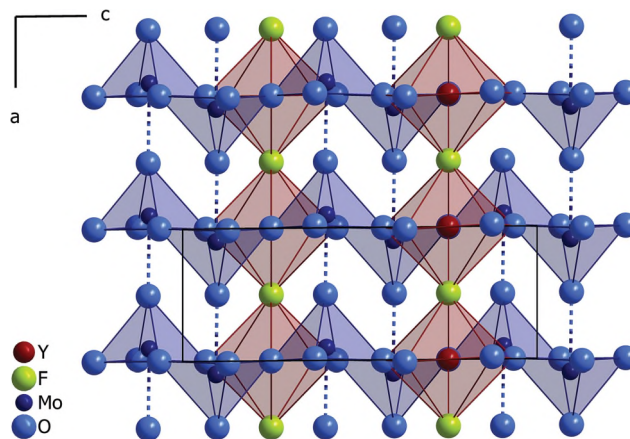


Fig. 5 View at the crystal structure of YFMO_2O_7 along the b -axis. While all the atoms are situated more or less on imaginary mirror planes at $x/a = 0$ and $1/2$, respectively, the Mo^{6+} cations reside about 0.4 Å offset.

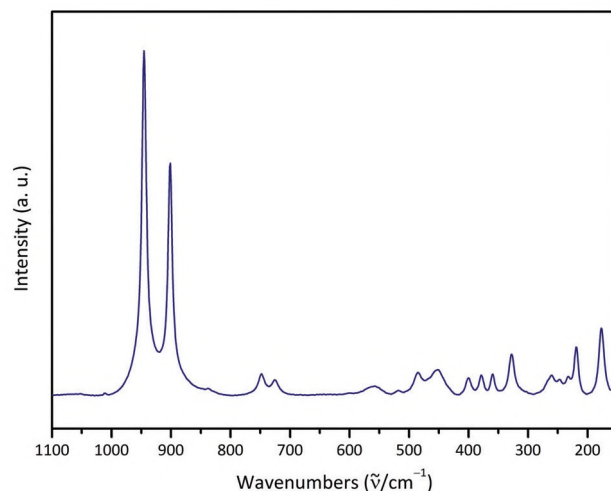
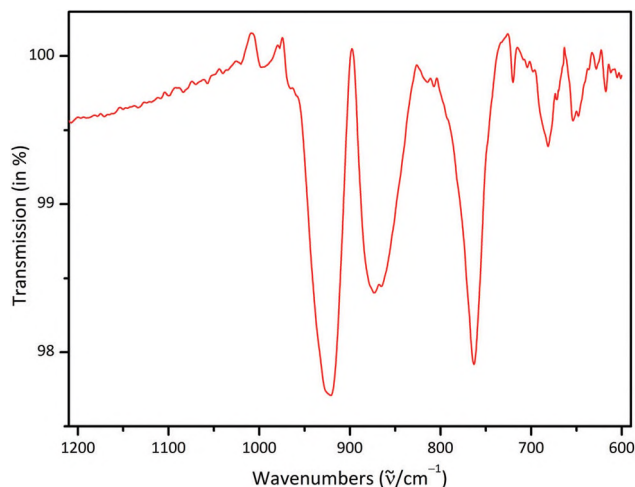


Fig. 6 Infrared (top) and Raman spectra (bottom) of YFMO_2O_7 .

numbers, which coincides well with another very wide band at about 760 cm^{-1} seen in the IR spectrum. In the Raman spectrum (Fig. 6, bottom) two very strong peaks at 945 and

901 cm^{-1} , respectively, are found, which can again be assigned to symmetric and asymmetric stretching vibrations, while the very weak ones between 700 and 800 cm^{-1} presumably also attribute to Mo–O and Mo–O–Mo stretching modes. The deformation vibrations of the oxidomolybdate(vi) units are expected well below 400 cm^{-1} , which cannot be detected in the IR spectrum due to device restrictions. These modes become visible in the Raman spectrum; however, in the supposed range below 400 cm^{-1} , but since Y–F and Y–O stretching modes are also present there, an explicit assignment of the peaks is not possible.

UV-Vis and photoluminescence spectroscopy

Yttrium(III) oxidomolybdates(vi) as well as their fluoride derivatives have already proven to be suitable host materials for luminescence-active lanthanoid(III) cations, such as Eu^{3+} .^{1,2} Doping experiments with the title compound have also been successful in yielding $\text{YFMo}_2\text{O}_7:\text{Eu}^{3+}$, which shows a bright red luminescence under UV irradiation ($\lambda_{\text{exc}} = 366 \text{ nm}$). In the emission spectrum the strongest peak at 612 nm (red curve in Fig. 7) is assigned to the ${}^5\text{D}_0 \rightarrow {}^7\text{F}_2$ electric dipole transition, because the Eu^{3+} cations, which substitute Y^{3+} at their crystallographically unique positions, are not located at an inversion center in the crystal structure. Hence, the ${}^5\text{D}_0 \rightarrow {}^7\text{F}_1$ magnetic dipole transition is also visible at 591 nm, displaying a minor contribution to the overall luminescence intensity.

The excitation spectrum (blue curve in Fig. 7) shows rather sharp signals at 393 and 464 nm, which are assigned to f–f transitions within the electronic valence shell of the Eu^{3+} cations. In such oxide-based compounds the top of the valence band is usually dominated by oxygen p states, while the bottom of the conduction band can be assigned to d states of the highly oxidized transition metal atom, providing the possibility of $\text{O}^{2-} \rightarrow \text{M}^{n+}$ charge transfer (CT) transitions.²⁰ Accordingly, a broad band with a maximum at 325 nm is visible, attributed to the $\text{O}^{2-} \rightarrow \text{Mo}^{6+}$ CT process in the oxidomolybdate(vi) partial structure as well as to the well-known $\text{O}^{2-} \rightarrow \text{Eu}^{3+}$ CT

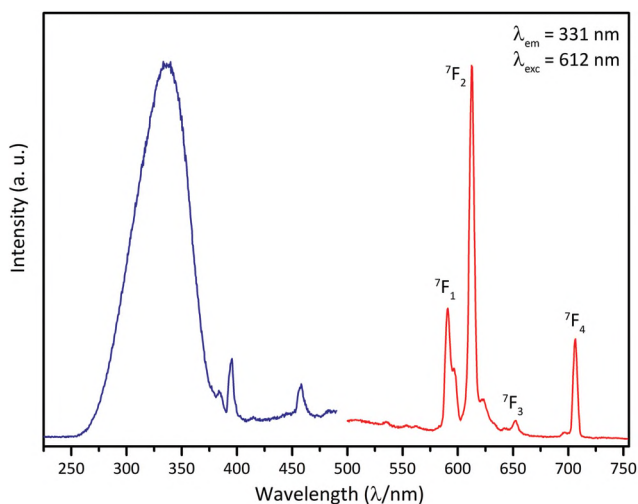


Fig. 7 Excitation (blue) and emission spectra (red) of $\text{YFMo}_2\text{O}_7:\text{Eu}^{3+}$.

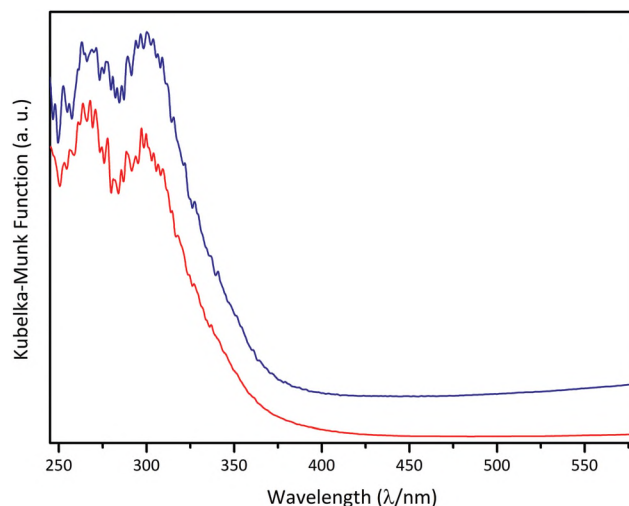


Fig. 8 Comparison of the diffuse UV-Vis reflectance spectra of YFMo_2O_7 (blue curve) with the Eu^{3+} -doped material (red curve).

transition. In the case of materials consisting of *ortho*-oxidomolybdate(vi) tetrahedra $[\text{MoO}_4]^{2-}$, the maximum of the $\text{O}^{2-} \rightarrow \text{Mo}^{6+}$ CT process is located at about 290 nm with little influence of the surrounding cationic situation.²¹ By enlarging the molybdate units by means of condensation (e.g. to $[\text{Mo}_2\text{O}_7]^{2-}$ anions) or enhancing the coordination number of Mo^{6+} from four to five (or even six) this maximum usually shifts towards regions of lower energy as seen in the spectrum of $\text{YFMo}_2\text{O}_7:\text{Eu}^{3+}$ compared to that of $\text{YF}[\text{MoO}_4]:\text{Eu}^{3+}$, where the maximum of the CT band lies at about 290 nm.² Unfortunately, it is not easy to distinguish the part of the $\text{O}^{2-} \rightarrow \text{Eu}^{3+}$ from the $\text{O}^{2-} \rightarrow \text{Mo}^{6+}$ CT process in the very wide charge transfer band. However, the position of the maximum can be attributed to the $\text{O}^{2-} \rightarrow \text{Mo}^{6+}$ CT, since the diffuse reflectance spectra of undoped YFMo_2O_7 and its Eu^{3+} -doped derivative are extremely similar (Fig. 8). In both spectra the onset point and the maximum of the optical band gap are found at about the same values ($\sim 380 \text{ nm}$ for the onset point and $\sim 325 \text{ nm}$ for the maximum) for the Eu^{3+} -doped and the undoped material, being in good agreement with the values determined from the excitation spectrum of $\text{YFMo}_2\text{O}_7:\text{Eu}^{3+}$ (Fig. 7, blue curve). Furthermore, this similarity also gives evidence to the statement that the main influence on the position of the broad charge transfer area in the excitation spectrum is dominated by the $\text{O}^{2-} \rightarrow \text{Mo}^{6+}$ rather than by the $\text{O}^{2-} \rightarrow \text{Eu}^{3+}$ CT transition. Thus, it appears that shifting this area towards the visible range of the electromagnetic spectrum is indeed possible by enlarging the oxidomolybdate units, either by condensation of tetrahedral $[\text{MoO}_4]^{2-}$ anions or by increasing the coordination number of the central Mo^{6+} cations.

Conclusions

The novel yttrium fluoride dimolybdate YFMo_2O_7 and its Eu^{3+} -doped derivative can be synthesized as phase-pure samples by

solid-state methods. The crystal structure does not consist of pyroanionic dimolybdate units ($[\text{Mo}_2\text{O}_7]^{2-}$), but of a layer-like arrangement of distorted $[\text{MoO}_{5+1}]^{6-}$ octahedra, which are fused together *via* common edges and vertices. Vibrational as well as optical spectroscopy investigations of both the Eu^{3+} -doped and undoped material were performed. It was possible to provide evidence on the shift of the optical band gap (with the $\text{O}^{2-} \rightarrow \text{Mo}^{6+}$ CT as its main part) towards lower energies being caused by the enlargement of the oxido-molybdate(vi) array.

Acknowledgements

The authors thank Dr. Sabine Strobel for measuring the diffuse reflectance spectra with the fluorescence spectrometer of Prof. Dr. Wolfgang Kaim (Institute for Inorganic Chemistry, University of Stuttgart, Germany). Furthermore, the financial support of the German Science Foundation (Deutsche Forschungsgemeinschaft, DFG, Bonn, Germany, project HO 4503/1-1) and the Federal States of Baden-Württemberg and Bavaria (Stuttgart and Munich, Germany) is gratefully acknowledged.

Notes and references

- 1 S. Laufer, S. Strobel, Th. Schleid, J. Cybinska, A.-V. Mudring and I. Hartenbach, *New J. Chem.*, 2013, **37**, 1919–1926.
- 2 Th. Schleid, S. Strobel, P. K. Dorhout, P. Nockemann, K. Binnemans and I. Hartenbach, *Inorg. Chem.*, 2008, **47**, 3728–3735.
- 3 G. Blasse and B. C. Grabmeier, *Luminescent Materials*, Springer-Verlag, Berlin, Heidelberg, 1994.
- 4 T. Schustereit, Th. Schleid and I. Hartenbach, *Z. Naturforsch.*, 2011, **66b**, 763–770.
- 5 C. J. Clark and D. Hall, *Acta Crystallogr., Sect. B: Struct. Crystallogr. Cryst. Chem.*, 1976, **32**, 1545–1547.
- 6 T. Roisnel and J. Rodriguez-Carvajal, in *Mater. Sci. Forum, Proceedings of the Seventh European Powder Diffraction Conference EPDIC 7*, ed. R. Delhez and E. J. Mittemeijer, Barcelona, 2000, pp. 118–123.
- 7 W. Herrendorf and H. Bärnighausen, *HABITUS: Program for the Optimization of the Crystal Shape for Numerical Absorption Correction in X-SHAPE (version 1.06, Fa. Stoe, Darmstadt 1999)*, Karlsruhe, Gießen, 1993, 1996.
- 8 G. M. Sheldrick, *Acta Crystallogr., Sect. A: Fundam. Crystallogr.*, 2008, **64**, 112–122.
- 9 *International Tables for Crystallography*, ed. Th. Hahn and A. J. C. Wilson, Kluwer Academic Publishers, Boston, Dordrecht, London, 2nd edn, 1992, vol. C.
- 10 R. X. Fischer and E. Tillmanns, *Acta Crystallogr., Sect. C: Cryst. Struct. Commun.*, 1988, **44**, 775–776.
- 11 (a) R. Hoppe, *Adv. Fluorine Chem.*, 1970, **6**, 387–438; (b) R. Hoppe, *Izv. Jugoslav. Centr. Krist. (Zagreb)*, 1973, **8**, 21–36; (c) R. Hoppe, in *Crystal Structure and Chemical Bonding in Inorganic Chemistry*, ed. C. J. M. Rooymans and A. Rabenau, Amsterdam, 1975, p. 127.
- 12 W. W. Wendlandt and H. G. Hecht, *Reflectance Spectroscopy*, Interscience Publishers, New York, 1966.
- 13 G. H. Dieke, *Spectra and Energy Levels of Rare Earth Ions in Crystals*, Interscience Publishers, New York, 1969.
- 14 A. Vadrine, J. P. Besse, G. Baud and M. Capestan, *Rev. Chim. Miner.*, 1970, **7**, 593–610.
- 15 M. G. Paton and E. N. Maslen, *Acta Crystallogr.*, 1965, **19**, 307–310.
- 16 B. M. Gatehouse and P. Leverett, *J. Chem. Soc. A*, 1969, **1969**, 849–854.
- 17 N. Wooster, *Z. Kristallogr.*, 1931, **80**, 504–512.
- 18 R. Hoppe, *Z. Kristallogr.*, 1979, **150**, 23–52.
- 19 G. Busca, *J. Raman Spectrosc.*, 2002, **33**, 348–358.
- 20 M. Daub, A. J. Lehner and H. A. Höpfe, *Dalton Trans.*, 2012, **41**, 12121–12128.
- 21 G. Blasse, *Struct. Bonding*, 1980, **42**, 1–41.